

**Appendix DR1: *Experimental Details and Sample Preparation***

We used an all solid-salt general shear sample assembly (Fig. DR1). Core and powdered samples had dimensions of  $\sim 1$  to  $2$  mm  $\times$   $\sim 6.3$  mm; slices of cores and cold-pressed powdered samples were enclosed in an inner Pt jacket and outer Ni jacket. Pt discs were placed between the yttria-stabilized ZrO<sub>2</sub> shear and axial pistons. NaCl was the confining medium for both the inner furnace and outer assembly. We measured temperature using a Pt-Pt10%Rh thermocouple centered on the sample outside the outer Ni jacket. Based on previous calibrations, the temperature varies by  $\sim 10$  °C along the sample, which is consistent with the homogeneous distribution of reaction phases observed in the sample. Stress is accurate to  $\pm 10$  MPa and corrected for the strain rate dependence of friction (for example, Chernak and Hirth, 2011).

Samples were annealed for approximately 24 hours prior to deformation (during  $\sigma_1$  piston advancement). We calculated shear stress versus shear strain curves using an initial thickness of the samples ( $\sim 1$  mm, based on the thickness of the hydrostatic sample) and the measured final sample thickness and shear displacement of the pistons. We corrected the force and displacement data to account for changes in sample/shear piston overlap during the experiment and axial shortening. Differential stress measurements were corrected for the effect of strain rate dependence of friction calibrated by strain rate stepping test at  $\dot{\epsilon} = 10^{-5} \text{ s}^{-1}$  and  $10^{-6} \text{ s}^{-1}$  during the sample run-in (i.e., before the deformation piston hit the sample). The data points used to determine the stress exponent were obtained from the strain rate stepping experiments (red and black curves, Fig. 3) and were corrected for friction (+18 MPa for  $10^{-6} \text{ s}^{-1}$  apparent strain rates, -18 MPa for  $10^{-4} \text{ s}^{-1}$  apparent strain rates).

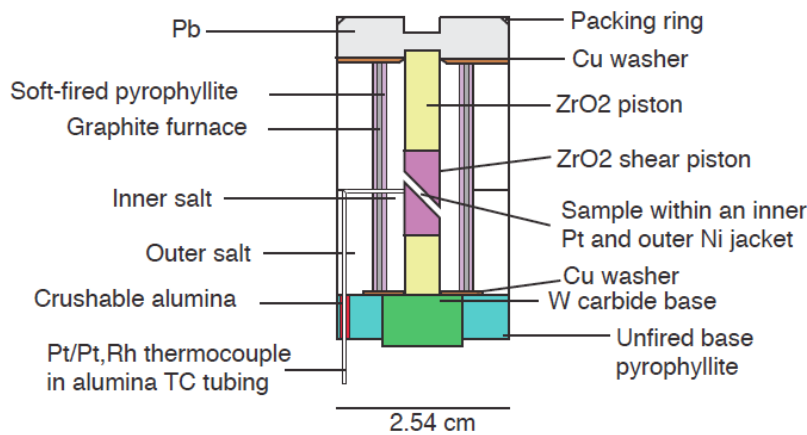


Figure DR1: Solid-salt general shear sample assembly. The shear pistons are inclined 45°.

## Appendix DR2: X-ray Diffraction (XRD)

We used XRD data to determine the amount of amphibole that formed during experiments and to compare to the measured phase abundances determined with EBSD data. The samples were first powdered using an agate mortar and pestle and then mounted in a Kapton® sample holder and inserted into a Terra® XRD diffractometer with Co  $K\alpha$  radiation and a cooled charge-coupled device (CCD) detector. Piezoelectric actuators shook the sample cell during analysis. Measurements were obtained between  $5^\circ$  and  $55^\circ 2\theta$  for  $\sim 1.25$  hours (only  $9^\circ$  to  $55^\circ 2\theta$  is shown in Fig. DR1 to eliminate the low  $2\theta$  peak associated with the Kapton® sample holder).

We used the fundamental-parameter Rietveld refinement method (Rietveld, 1969) to model the measured XRD data and to estimate mineral abundances. All backgrounds were modeled using a third-order Chebyshev polynomial. Refined parameters included unit-cell parameters, specimen crystallite size and strain, second- to fourth-order spherical harmonics for preferred orientation correction, scaling factor, and mineral abundance. Phases included in the refinement were anorthite (Klein and Korekawa, 1976), diopside (Cameron et al., 1973), olivine (Miyake et al., 1987), hornblende (Phillips et al., 1989; Makino and Tomita, 1989), enstatite (Hugh-Jones and Angel, 1994), and quartz (Levien et al., 1980). The Rietveld refinement results are shown in Figure DR2, and the unit cell parameters are listed in Table T1A.

These XRD data clearly demonstrate that the prominent amphibole peaks at  $11.4^\circ$ ,  $12.3^\circ$ , and  $38.6^\circ 2\theta$  present in the deformed, hydrated basalt (Fig. DR1b) are not observed in the basalt starting material (Fig. DR1a). The phase percentages are similar to those estimated using EBSD percentages of phases indexed.

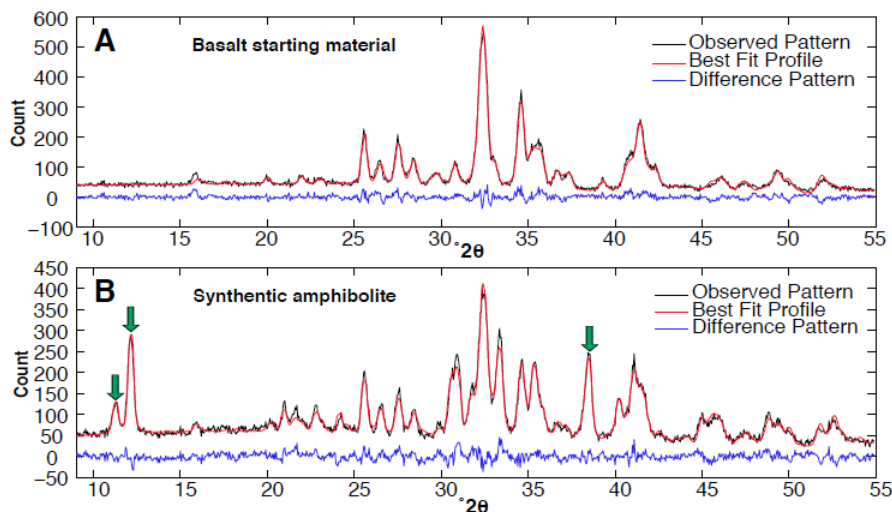


Figure DR2: XRD data for A) the starting basalt powder and B) experimental amphibolite (experiment W1772). Observed profile (black), best-fit Rietveld refinement profile (red), and difference pattern (blue) are shown. Green arrows point to amphibole peaks 020 ( $2\theta = 11.4^\circ$ ), 110 ( $2\theta = 12.3^\circ$ ), and 151 ( $2\theta = 38.6^\circ$ ), all of which are present in B but not A. Peak positions are relative to the cobalt X-ray source.

**Table DR1.** Space group, unit cell parameters,  $R_{wp}$ , and phase percentages obtained from XRD analysis.

Basalt Starting Material ( $R_{wp} = 12.197$ )		Anorthite	Amphibole	Diopside	Enstatite	Forsterite	Chlorite	Quartz
Space Group		C-1	C12/m1	C12/c1	Pbca	Pbnm	C2/m	P3221
a (Å)		8.17	9.87	9.81	18.04	4.81	5.35	4.79
b (Å)		12.88	17.98	8.94	8.83	10.30	9.03	-
c (Å)		14.25	5.19	5.31	5.29	6.03	14.17	5.42
alpha		93.46	-	-	-	-	-	-
beta		116.20	105.20	106.09	-	-	96.29	-
gamma		89.95	-	-	-	-	-	-
%		52.90	0.40	31.10	1.80	11.60	1.70	0.40
W1772 ( $R_{wp} = 10.660$ )								
Space Group		C-1	C12/m1	C12/c1	Pbca	Pbnm	C2/m	P3221
a (Å)		8.15	9.79	9.76	18.20	4.77	5.18	4.92
b (Å)		12.82	18.06	8.92	8.73	10.11	9.45	-
c (Å)		14.17	5.31	5.28	5.30	6.13	14.39	5.36
alpha		93.62	-	-	-	-	-	-
beta		116.16	104.84	106.15	-	-	96.68	-
gamma		89.87	-	-	-	-	-	-
%		31.40	45.90	13.80	0.50	2.00	3.30	3.20

**Appendix DR3: Clinopyroxene LPO**

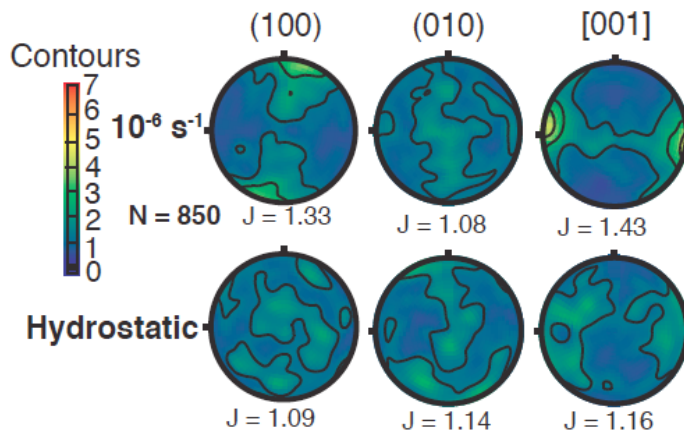


Figure DR3: Pole figures quantifying the LPO for clinopyroxene in fine-grained experimental amphibolite. Top row: the deformed experimental amphibolite (W1772) showing a weak clinopyroxene LPO. Bottom row: the hydrostatic experimental amphibolite (W1779) showing a random clinopyroxene LPO. J quantifies the fabric strength (J-index; Mainprice and Silver, 1993). Mean angular deviation number for all experimental samples is  $< 0.8$ . Contours are multiples of a uniform distribution. Shear sense is sinistral in A. All plots are lower-hemisphere projections contoured with a  $15^\circ$  half-width using the software of D. Mainprice ([ftp://www.gm.univ-montp2.fr/mainprice//CareWare\\_Unicef\\_Programs/](ftp://www.gm.univ-montp2.fr/mainprice//CareWare_Unicef_Programs/)).

## REFERENCES

- Cameron, M., Sueno, S., Prewitt, C.T., and Papike, J.J., 1973, High-temperature crystal chemistry of acmite, diopside, hedenbergite, jadeite, spodumene, and ureyite: *The American Mineralogist*, v. 58, p. 594–618.
- Chernak, L.J., and Hirth, G., 2011, Syndeformational antigorite dehydration produces stable fault slip: *Geology*, v. 39, no. 9, p. 847–850, doi:10.1130/G31919.1.
- Hugh-Jones, D.A., and Angel, R.J., 1994, A compressional study of MgSiO<sub>3</sub>, orthoenstatite up to 8.5 GPa: *The American Mineralogist*, v. 79, no. 5–6, p. 405–410.
- Klein, S., and Korekawa, M., 1976, Die gemittelte Struktur des Labradorits: *N Jahrb Mineral Monatsh*, p. 66–69.
- Levien, L., Prewitt, C.T., and Weidner, D.J., 1980, Structure and elastic properties of quartz at pressure: *The American Mineralogist*, v. 65, no. 9–10, p. 920–930.
- Makino, K., and Tomita, K., 1989, Cation distribution in the octahedral sites of hornblendes: *The American Mineralogist*, v. 74, no. 9–10, p. 1097–1105.
- Miyake, M., Nakamura, H., Kojima, H., and Marumo, F., 1987, Cation ordering in Co-Mg olivine solid-solution series: *The American Mineralogist*, v. 72, p. 594–598.
- Phillips, M.W., Draheim, J.E., Popp, R.K., Clowe, C.A., and Pinkerton, A.A., 1989, Effects of oxidation-dehydrogenation in tschermakitic hornblende: *The American Mineralogist*, v. 74, no. 7–8, p. 764–773.
- Rietveld, H., 1969, A profile refinement method for nuclear and magnetic structures: *Journal of Applied Crystallography*, v. 2, no. 2, p. 65–71, doi:10.1107/S0021889869006558.